Learning Semantic and Visual Similarity for Endomicroscopy Video Retrieval

Barbara André, Tom Vercauteren, Anna M. Buchner, Michael B. Wallace, and Nicholas Ayache

***Abstract*—Content-Based Image Retrieval (CBIR) is a valuable computer vision technique which is increasingly being applied in the medical community for diagnosis support. However, traditional CBIR systems only deliver visual outputs, i.e. images having a similar appearance to the query, which is not directly interpretable by the physicians. Our objective is to provide a system for endomicroscopy video retrieval which delivers both visual and semantic outputs that are consistent with each other. In a previous study, we developed an adapted bag-of-visual-words method for endomicroscopy retrieval, called "Dense-Sift", that computes a *visual* signature for each video. In this study, we present a novel approach to complement visual similarity learning with semantic knowledge extraction, in the field of *in vivo* endomicroscopy. We first leverage a semantic ground truth based on 8 binary concepts, in order to transform these *visual* signatures into *semantic* signatures that reflect how much the presence of each semantic concept is expressed by the visual words describing the videos. Using cross-validation, we demonstrate that, in terms of semantic detection, our intuitive Fisher-based method transforming visual-word histograms into semantic estimations outperforms Support Vector Machine (SVM) methods with statistical significance. In a second step, we propose to improve retrieval relevance by learning an adjusted similarity distance from a perceived similarity ground truth. As a result, our distance learning method allows to statistically improve the correlation with the perceived similarity. We also demonstrate that, in terms of perceived similarity, the recall performance of the *semantic* signatures is close to that of *visual* signatures and significantly better than those of several state-of-the-art CBIR methods. The *semantic* signatures are thus able to communicate high-level medical knowledge while being consistent with the low-level *visual* signatures and much shorter than them. In our resulting retrieval system, we decide to use *visual* signatures for perceived similarity learning and retrieval, and *semantic* signatures for the output of an additional information, expressed in the endoscopist own language, which provides a relevant semantic translation of the visual retrieval outputs.**

***Index Terms*—Content-Based Image Retrieval, Bag-of-Visual-Words, Semantic and Visual Similarity, Similarity Learning, Semantic Gap, Endomicroscopy**

I. Introduction

The Content-Based Image Retrieval (CBIR) techniques, inherited from the computer vision field, have various medical applications. Müller et al. [1] presented a benchmark for the evaluation of multimodal CBIR methods on medical databases according to the "ImageCLEF" medical image retrieval task that includes heterogeneous medical images, from radiography and electrocardiograms to histopathology. More recently, a dense CBIR approach was proposed by Avni et al. [2]

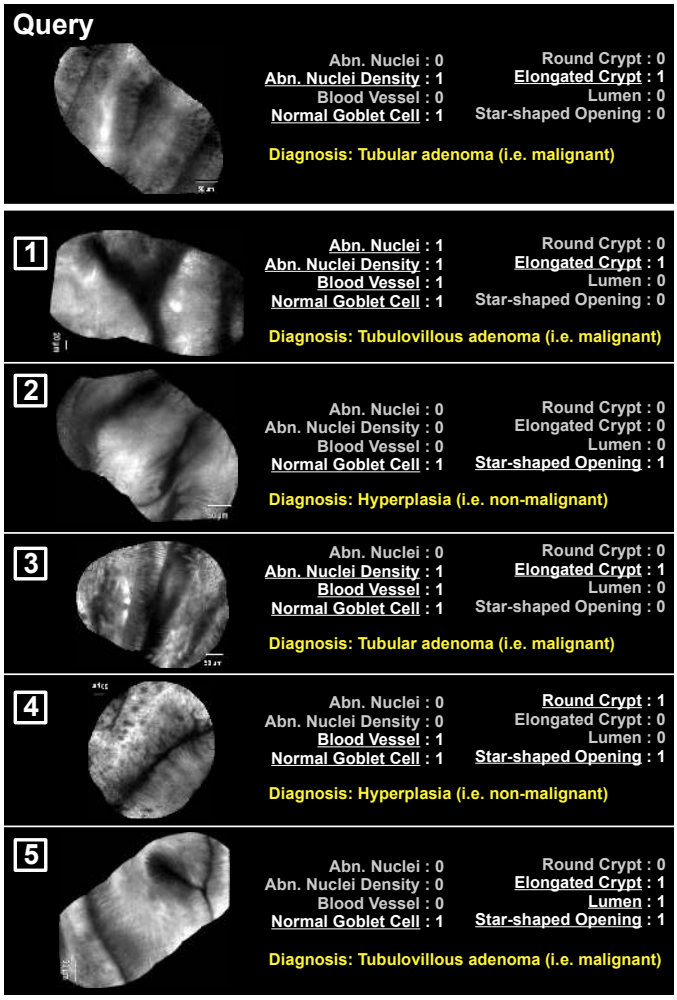

Fig. 1: Illustration of the semantic gap: content-based retrieval of visually similar pCLE videos having dissimilar semantic annotations. The 5 most similar pCLE videos are retrieved by the "Dense-Sift" method that only relies on visual features. The semantic concepts annotated as present in a given video are underlined and set to 1, those annotated as absent are set to 0. For each video, the pathological diagnosis, either malignant or non-malignant, is indicated below the semantic concepts. For illustration purposes, videos are represented by mosaic images.

B. André and T. Vercauteren are with the company Mauna Kea Technologies, Paris, France, E-mails: barbara.andre@maunakeatech.com, tom.vercauteren@maunakeatech.com

A.M. Buchner is with the Hospital of the University of Pennsylvania, Philadelphia, US, E-mail: anna.buchner@uphs.upenn.edu

M.B. Wallace is with the Mayo Clinic of Jacksonville, Florida, US, E-mail: Wallace.Michael@mayo.edu

N. Ayache is with the Asclepios Research Team at INRIA - Sophia Antipolis, France, E-mail: nicholas.ayache@sophia.inria.fr

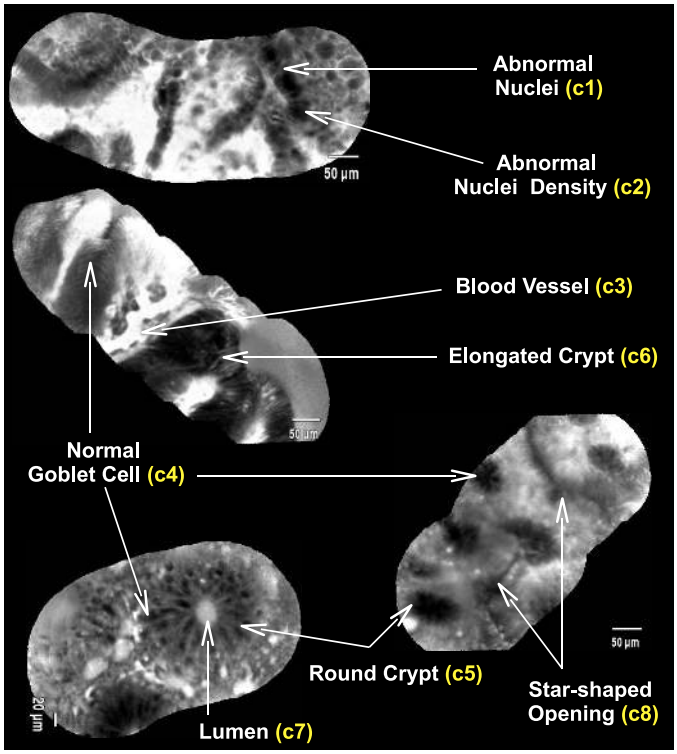

Fig. 2: Examples of training pCLE videos represented by mosaic images and annotated with the 8 semantic concepts. The two mosaics on the top show neoplastic (i.e. malignant) colonic polyps, while the two mosaics on the bottom show non-neoplastic (i.e. non-malignant) colonic polyps. On the left, the mosaics from top to bottom were respectively built using 12, 6 and 10 frames. On the right, the mosaic was built using 27 frames. The size of a mosaic does not only depend on the number of frames used to build it, but also on the motion velocity of the probe during pCLE imaging.

for organ-level and pathology-level categorization of x-ray images. The expanding application of CBIR methods in the medical diagnosis field faces the semantic gap, which was pointed out by Smeulders et al. in [3] and by Akgül et al. in [4], as a critical issue. The semantic gap in CBIR is the disconnection between the reproducible computational representation of low-level visual features in images and the context-dependent formulation of high-level knowledge, or semantics, to interpret these images. Two medical images being highly similar in appearance may have contradictory semantic annotations. So a CBIR system, which would be only based on visual content, might lead the physician toward a false diagnosis. Conversely, two medical images having exactly the same semantic annotations may look visually dissimilar. So a CBIR system, for which the semantics of the query is unknown, might not retrieve all clinically relevant images. In fact, when interpreting a new image for diagnostic purposes, the physician uses similarity-based reasoning, where *similarity* includes both visual features and semantic concepts. To mimic this process, we aim at capturing the visual content of images using the Bag-of-Visual-Words (BoW) method, and at estimating the expressive power of visual words with respect to multiple semantic concepts. This leads us to compute semantic estimations which have the potential to provide the physician with a relevant semantic translation of the retrieval results.

Our medical application is the retrieval of probe-based Confocal Laser Endomicroscopy (pCLE) videos to support the early diagnosis of colonic cancers. pCLE is a recent imaging technology that enables the endoscopist to acquire *in vivo* microscopic video sequences of the epithelium, at a rate of 9 to 18 frames per second, and thus to establish a diagnosis in real time. In particular, the *in vivo* diagnosis of colonic polyps using pCLE is still challenging for many endoscopists, because of the high variability in the appearance of pCLE videos and the presence of atypical cases such as serrated adenoma [5]. Examples of mosaic images extracted from pCLE videos are shown in Fig. 1 which also provides an illustration of the semantic gap in endomicroscopy retrieval. In [6] we have developed a dense BoW method, called "Dense-Sift", for the content-based retrieval of pCLE videos. We showed that, when evaluated in terms of pathological classification of pCLE videos, "Dense-Sift" significantly outperforms several state-of-the-art CBIR methods. Parts of this paper are extensions of a preliminary study [7] where we explored pCLE retrieval evaluation and distance learning in terms of perceived visual similarity. In this study, we present a novel approach to bridge the gap between visual pCLE features and semantic pCLE knowledge. Our objective is to extract semantic information as an additional information that complements the visual outputs of our CBIR method, in order to provide the endoscopists with semantic insight into the retrieval results. A primary version of this paper can be found in our research report [8].

To this purpose, we consider two types of ground truth presented in Section II: the first type contains visual similarities perceived by endoscopists between pCLE videos, evaluated on a four-point Likert scale, and the second type contains eight binary semantic concepts which are commonly used by expert endoscopists to diagnose pCLE videos of colonic polyps. These semantic concepts are illustrated in Fig. 2. In Section III we briefly described our "Dense-Sift" retrieval method. From the *visual* signatures computed by "Dense-Sift" and from the semantic ground truth, we build visual-word-based *semantic* signatures using a Fisher-based approach detailed in Section IV. We evaluate the relevance of the resulting *semantic* signatures, first from the semantic point of view, with ROC curves showing detection performances for each semantic concept, and then from the perceptual point of view, with *sparse recall* curves showing the ability of the induced *semantic* distance to capture video pairs perceived as *very similar*. In order to improve retrieval relevance, we propose in Section V a method to learn an adjusted similarity distance from the perceived similarity ground truth. A linear transformation of video signatures is optimized, that minimizes a margin-based cost function differentiating *very similar* video pairs from the others. The results shown in Section VI show that the visual-word-based *semantic* signatures yield a recall performance which is slightly lower than that of the original *visual* signatures computed by "Dense-Sift", but significantly higher than those of several state-of-the-art methods in CBIR. In terms of correlation with the perceived similarity, the retrieval performance of *semantic* signatures is

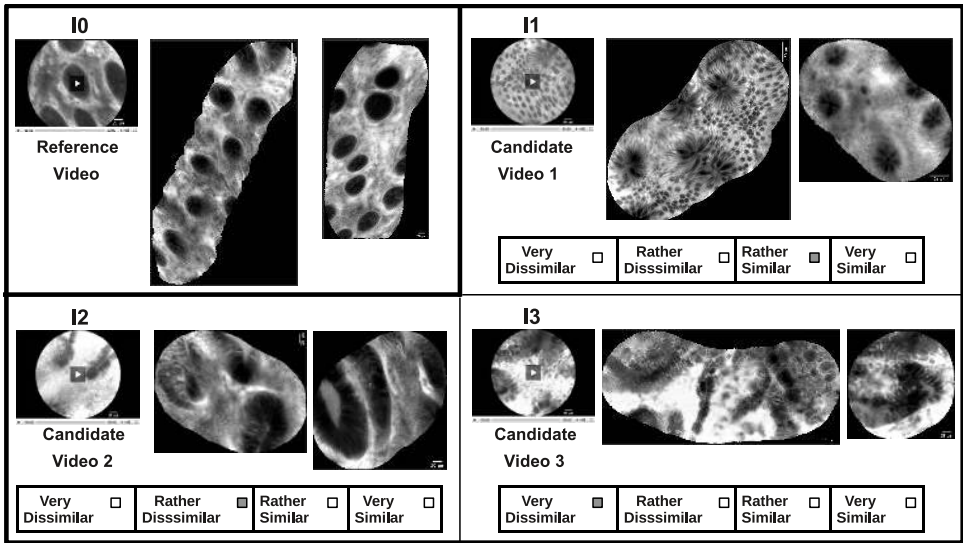

Fig. 3: Schematic outline of the online "Visual Similarity Scoring" tool showing the example of a scoring process, where 3 video couples (I_0, I_1), (I_0, I_2) and (I_0, I_3) are proposed. Each video is summarized by a set of mosaic images, two of which are shown here as an example.

better, with statistical significance, than those of the state-of-the-art methods, and comparable to that of the original *visual* signatures. For both *semantic* signatures and *visual* signatures, the distance learning method allows to improve, with statistical significance, the correlation with the perceived similarity. Our resulting pCLE retrieval system, of which visual and semantic outputs are consistent with each other, should better assist the endoscopist in establishing a pCLE diagnosis.

II. Ground Truth for Perceived Visual Similarity and for Semantics

A. pCLE database

Our video database contains 118 pCLE videos of colonic polyps that were acquired from 66 patients for the study of Buchner et al. [9]. The lengths of the acquired pCLE videos range from 1 second to 4 minutes, depending on the time spent to image the lesion of interest. All the patients underwent a surveillance colonoscopy with pCLE for fluorescein-aided imaging of suspicious colonic polyps before their removal. For each patient, pCLE was performed of each detected polyp with one video corresponding to each particular polyp. All polyps were removed and evaluated by a pathologist to establish the "gold standard" diagnosis.

During the colonoscopy procedures the pCLE miniprobe was in constant contact with the epithelium, so the viewpoint changes between the images of stable pCLE video sequences are mostly in-plane rotations and translations. For this reason, we can represent any pCLE video as a set of mosaic images built with the video-mosaicing technique of Vercauteren et al. [10], each mosaic image corresponding to a stable subsequence of the video. pCLE mosaic images will not only be used as input for our retrieval system, but also as retrieval output attached to the extracted similar videos. Indeed, Dabizzi et al. [11] recently showed that pCLE mosaics have the potential to replace pCLE videos for a comparable diagnosis accuracy and a significantly shorter interpretation time.

B. Ground Truth for Perceived Visual Similarity

To generate a pairwise similarity ground truth between pCLE videos, we designed an online survey tool, called VSS [12], that allows multiple observers, who are fully blinded to the video metadata such as the pCLE diagnosis, to qualitatively estimate the perceived visual similarity degree between videos. The VSS tool proposes, for each video couple, the following four-point Likert scale: *very dissimilar*, *rather dissimilar*, *rather similar* and *very similar*. Because interpreting whole video sequences is time consuming, the VSS supports this task by making available both the whole video content and for each video, its set of static mosaic images providing a visual summary. Each scoring process, as illustrated in Fig. 3, is characterized by the random drawing of 3 video couples (I_0, I_1), (I_0, I_2) and (I_0, I_3), where the candidate videos I_1, I_2 and I_3 belong to patients that are different from the patient of the reference video I_0, in order to exclude any patient-related biases. 17 observers, ranging from middle expert to expert in pCLE diagnosis, performed as many scoring processes as they could. Our generated ground truth can be represented as a weighted oriented graph $G = (V, E)$ where the nodes in V are the videos and where each couple of videos may be connected by zero, one or several edges in E weighted by the similarity scores. As less than 2% of these video couples were scored by more than 2 distinct observers, it was not relevant to measure inter-observer variability. In total, $4,836$ similarity scores were given for $2,178$ distinct video couples. Thus 16.2% of all $13,434$ distinct video couples were scored. Compared to our preliminary study [7] where 14.5% of all possible video couples were scored, the perceived similarity ground truth was enriched for this study in order to better differentiate potentially *very similar* video pairs from

the others, a goal which is closer to our retrieval purpose.

If the video couples were randomly drawn with a uniform non-informative prior by the VSS tool, we would have drawn many more video pairs perceived as *dissimilar* than video pairs perceived as *very similar*. The resulting perceived similarity ground truth would have been too far from our clinical application which aims at extracting highly visually similar videos. For this reason, we use the *a priori* similarity distance d_{Vis} computed by the "Dense-Sift" method to enable two modes for the drawing of video pairs: in the first mode, video pairs with different perceived similarities are equally likely to be drawn; in the second mode, video pairs perceived as *very similar* are more likely to be drawn. Using this *a priori* distance can deliver a slight bias in the VSS process, however it is an efficient solution to increase the number of *very similar* video pairs.

More precisely, in the first mode, the probability of drawing a video couple (I_i, I_j) is proportional to the inverse of the density of $d_{prior}(I_i, I_j)$. In the second mode, the video I_j is one of the 5 nearest neighbors of the video I_i according to the retrieval distance d_{Vis}. A total of $3,801$ similarity scores was recorded with the first mode, and $1,035$ with the second mode.

Although the resulting similarity graph remains very sparse, we will show in Section VI that it constitutes a valuable ground-truth database for retrieval evaluation and for perceived similarity learning.

C. Ground Truth for Semantic Concepts

All the acquired pCLE videos were manually annotated with $M = 8$ binary semantic concepts that are illustrated on pCLE mosaic images in Fig. 2. The eight semantic concepts were defined by the endoscopists, who use them as main criteria to diagnose the colonic polyps from pCLE videos. These semantic concepts express a mid-level clinical knowledge, which we consider as "high-level" clinical knowledge in contrast to the low-level visual features. As pCLE images are rather new for many endoscopists, the taxonomy of pCLE semantics is still under construction. Although eight semantic concepts is a relatively small number, it is a first necessary step for the full understanding of the pathologies observed in pCLE videos. In a given pCLE video, each semantic concept is defined as either visible, potentially several times, or not visible at all in the video. The first two concepts, *abnormal nuclei* (c_1) and *abnormal nuclei density* (c_2), which are the most difficult to identify, were annotated by two expert endoscopists. With the support of the modified Mainz criteria identified by Kiesslich et al. [13] six other concepts were annotated: *blood vessel* (c_3), *normal goblet cell* (c_4), *round crypt* (c_5), *elongated crypt* (c_6), *lumen* (c_7) and *star-shaped opening* (c_8). If the semantic j^{th} concept is visible in the video then $c_j = 1$ else $c_j = 0$. Table I shows, for each semantic concept, the percentage of the videos in the database where the concept is annotated as visible.

Semantic concept	**Frequency**
c1. abnormal nuclei	46.6 %
c2. abnormal nuclei density	63.6 %
c3. blood vessel	47.5 %
c4. normal goblet cell	72.0 %
c5. round crypt	47.5 %
c6. elongated crypt	64.4 %
c7. lumen	27.1 %
c8. star-shaped opening	18.6 %

TABLE I: Frequency of each semantic concept. The frequency of each semantic concept is measured by the percentage of the videos in the database where the concept is annotated as visible.

III. From pCLE Videos to Visual Words

Among the state-of-the-art methods in CBIR, the BoW method of Zhang et al. [14], referred to as "HH-Sift", is particularly successful for the retrieval of texture images in computer vision. Whereas "HH-Sift" combines the sparse "Harris-Hessian" detector with the SIFT descriptor, the "Textons" method proposed by Leung and Malik [15] is based on a dense description of local texture features. Adjusting these approaches for pCLE retrieval, we proposed in [6] the "Dense-Sift" method with the following parameters: disk regions of radius 60 pixels, a total of $K = 100$ visual words and dense SIFT description of explicit mosaic images. In the field of computer vision, the superiority of the dense SIFT descriptor, compared to the standard sparse SIFT descriptor, was demonstrated by Li and Perona for natural scene classification in [16]. The image description performed by our "Dense-Sift" method is invariant to in-plane rotations and in-plane translations changes that are due to the motion of the pCLE miniprobe, and to the affine illumination changes that are due to the leakage of fluorescein used in pCLE. "Dense-Sift" also enables the extension from pCLE image description to pCLE video description by leveraging video mosaicing results. As a result, "Dense-Sift" computes a visual word signature $\mathscr{S}_{\text{Vis}}(I) = (w_1^I, ..., w_K^I)$ for each pCLE video I, where w_k^I is the frequency of the k^{th} visual word in the video I. We define the visual similarity distance $d_{\text{Vis}}(I, J)$ between two videos I and J as the χ^2 pseudo-distance between their visual word signatures computed by "Dense-Sift":

$$\begin{aligned} d_{\text{Vis}}(I,J) &= \chi^2(\mathscr{S}_{\text{Vis}}(I), \mathscr{S}_{\text{Vis}}(J)) \\ &= \frac{1}{2} \sum_{k\in\{1,..,K\}, w_k^I w_k^J > 0} \frac{(w_k^I - w_k^J)^2}{w_k^I + w_k^J} \end{aligned} \quad (1)$$

The last CBIR method which we consider as a reference is the "Haralick" [17] method based on global statistical features. We use an extended Haralick method, provided by Avinash Uppuluri in Matlab Central [18], that extracts 23 texture features computed from the Gray Level Co-occurrence Matrices (GLCM). The seminal method of Haralick consists of extracting 13 global statistical features from the co-occurrence matrix which is computed on the whole image at the first level of adjacency. Other global descriptors have been proposed more recently in the literature, such as the gist descriptor of Oliva and Torralba [19].

Among the four state-of-the-art CBIR methods, "HH-Sift", "Textons", "Dense-Sift" and "Haralick", our "Dense-Sift" method was proven in [6] to be the best method in terms of

pathological classification of pCLE videos. "Dense-Sift" will also be proven to be the best method in terms of correlation with the perceived visual similarity, as shown in Section VI. For these reasons, we decided to build the *semantic* signatures of pCLE videos from the *visual* signatures computed by "Dense-Sift".

IV. From Visual Words to Semantic Signatures

Among the approaches in bridging the semantic gap, recent methods based on random-walk processes on visual-semantic graphs were proposed by Poblete et al. [20] and by Ma et al. [21]. Latent semantic indexing approaches have also been investigated, for example by Caicedo et al. [22] to improve medical image retrieval. Rasiwasia et al. [23], [24] proposed a probabilistic method which we consider as a reference method for performing a semantic retrieval which is based on visual features. In particular, their approach estimates for each semantic concept the probability that, given a visual feature vector in an image, the semantic concept is present in the image. In [25], Kwitt et al. recently applied this method for learning pit pattern concepts in endoscopic images of colonic polyps. These pit pattern concepts at the macroscopic level can be seen as corresponding to our semantic concepts at the microscopic level. In order to learn semantic concepts from visual words in endomicroscopic videos, we propose a rather simple method providing satisfactory results. The application of a probabilistic method such as the one in [23] on our data was not successful, certainly because of our relatively small sample size, but we plan to further investigate it. Our proposed method is a Fisher-based approach that estimates the expressive power of each of the K visual words with respect to each of the M semantic concepts.

Let D^{train} be the set of training videos. Given the k^{th} visual word and the j^{th} semantic concept, we estimate the discriminative power of the k^{th} visual word with respect to the j^{th} semantic concept using the *signed* Fisher criterion:

$$F_{k,j} = \frac{\mu_1(k,j) - \mu_0(k,j)}{\sigma_1^2(k,j) + \sigma_0^2(k,j)} \tag{2}$$

where $\mu_p(k,j)$ (resp. $\sigma_p^2(k,j)$) is the mean (resp. the variance) of $\{w_k^I,\ c_j^I = p,\ I \in D^{train}\}$ with $p = 0$ or $p = 1$. We call F the resulting matrix of Fisher's weights. Given a video I with the *visual* signature $\mathscr{S}_{\text{Vis}}(I) = (w_1^I, ..., w_K^I)$, we define the *semantic weight* of I with respect to the j^{th} semantic concept as the following linear combination: $s_j^I = \sum_{k=1}^{K} F_{k,j} w_k^I$. Thus, the transformation from the *visual* signature $\mathscr{S}_{\text{Vis}}(I)$ into its visual-word-based *semantic* signature $\mathscr{S}_{\text{Sem}}(I) = (s_1^I, ..., s_M^I)$ is given by the equation:

$$\mathscr{S}_{\text{Sem}}(I) = F^T \mathscr{S}_{\text{Vis}}(I) \tag{3}$$

The signed value s_j^I reflects how much the presence of the j^{th} semantic concept is expressed by the visual words describing the video I. Finally, a visual-word-based *semantic* similarity distance between two videos I and J can be defined for example using the L^2 norm:

$$d_{\text{Sem}}(I,J) = ||\mathscr{S}_{\text{Sem}}(I) - \mathscr{S}_{\text{Sem}}(J)||_{L^2} \tag{4}$$

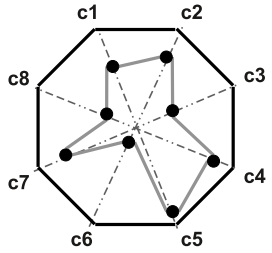

Fig. 4: An example of a star plot based on the 8 semantic concepts. The coordinate value along the j^{th} radius corresponds to the normalized value of the *semantic* signature at the j^{th} concept.

It thus becomes possible to use our short *semantic* signature of size $M = 8$ in order to retrieve pCLE videos that are the closest to a video query according to the *semantic* distance d_{Sem}. In Section VI we demonstrate that, in terms of correlation with the perceived visual similarity, the retrieval performance of the *semantic* distance d_{Sem} is comparable to that of the visual distance d_{Vis}.

In order to provide the endoscopists with a qualitative visualization of *semantic* signatures, we provide an intuitive and generic representation of any *semantic* signature using a star plot of M radii, as shown in Fig. 4. Given a video I and the j^{th} semantic concept, we normalize the *semantic weight* s_j^I into $(s_j^I - \min\{s_j^J, J \in D^{train}\})/(\max\{s_j^J, J \in D^{train}\} - \min\{s_j^J, J \in D^{train}\})$ in order to obtain the coordinate value of I along the j^{th} radius of the star plot. For example, in Fig. 5 the star plots represent, from some tested videos, the visual-word-based *semantic* signatures that have been learned from annotated training videos, such as the ones shown in Fig. 2.

V. Distance Learning from Perceived Similarity

Similarity distance learning has been investigated by recent studies to improve classification or recognition methods. Yang et al. [26] proposed a boosted distance metric learning method that projects images into a Hamming space where each dimension corresponds to the output of a weak classifier. Weinberger and Saul [27] explored convex optimizations to learn a Mahalanobis transformation such that distances between nearby images are shrunk if the images belong to the same class and expanded otherwise. At the level of image descriptors, Philbin et al. [28] have a similar approach that transforms the description vectors into a space where the clustering step more likely assigns matching descriptors to the same visual word and non-matching descriptors to different visual words.

In order to improve the relevance of pCLE retrieval, our objective is to shorten the distances between *very similar* videos and to enlarge the distances between non-*very similar* videos. As the approach of Philbin et al. [28] is closer to our pairwise visual similarity ground truth, we propose a generic distance learning technique inspired from their method. We aim at finding a linear transformation matrix W which maps given video signatures to new signatures that better discriminate *very similar* video pairs from the other video pairs. We thus consider two groups: D_+ is the set of N_+ training video

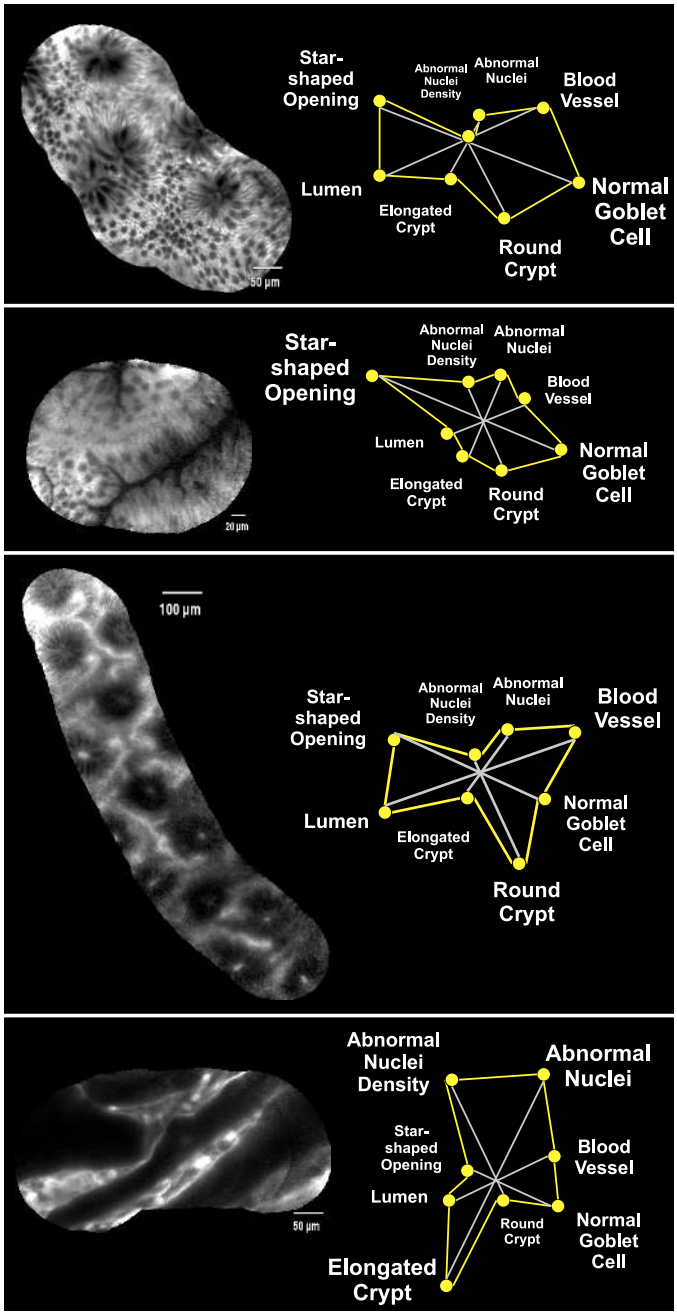

Fig. 5: Examples of tested pCLE videos, represented by mosaic images, and visualization of their learned *semantic* signatures using the star plot, as explained in Fig. 4. The font size of each written semantic concept is proportional to the value of the concept coordinate in the star plot. Underlined concepts are those which were annotated as present in the semantic ground truth. From top to bottom, the first three mosaics show non-neoplastic (i.e. non-malignant) colonic polyps and the fourth mosaic shows a neoplastic (i.e. malignant) colonic polyp.

couples that have been scored with $+2$ and D_- is the set of N_- training video couples that have been scored with $+1$, -1 or -2. We optimize the transformation W by minimizing the following margin-based cost function f:

$$f(W,\beta,\gamma) = \frac{1}{N+}\sum_{(I,J)\in D_+} g(\beta - d(W\ \mathscr{S}(I), W\ \mathscr{S}(J))) + \gamma\ \frac{1}{N_-}\sum_{(I,J)\in D_-} g(d(W\ \mathscr{S}(I), W\ \mathscr{S}(J)) - \beta) \quad (5)$$

where $\mathscr{S}(I)$ is the signature of the video I, $d(.,.)$ is the chosen distance between the video signatures, e.g. L^2 or χ^2, and $g(z) = log(1+e^{-z})$ is the logistic-loss function. The cost function f has the three following parameters: the transformation matrix W, the margin β and the constant parameter γ that potentially penalizes either non-*very similar* nearby videos or *very similar* remote videos. We could optimize f with respect to all 3 parameters, but this would make the search for the optimum more sensitive to local minima. We therefore decide to fix the value of the margin β using an intuitive heuristic: we take as a relevant value for β the threshold on the distances between video signatures that maximizes the classification accuracy between D_+ and D_-. All possible values of the parameter γ are then discretized into a finite number of values, at which the cost function f is optimized according to W. As long as the distance $d(.,.)$ is differentiable, f can be differentiated with respect to W. Given a pCLE video I, its signature $\mathscr{S}(I)$ of size X is mapped to the transformed signature $W^{opt}\ \mathscr{S}(I)$, where W^{opt} is the optimized transformation matrix of size $X \times X$. The learned similarity distance between two pCLE videos I and J is then defined as:

$$d^{learn}(I,J) = d(W^{opt}\mathscr{S}(I), W^{opt}\mathscr{S}(J))) \quad (6)$$

The application of this generic distance learning scheme to the *semantic* signatures of size $X = 8$ is straightforward: the transformation matrix W is of size $X \times X = 64$, $\mathscr{S} = \mathscr{S}_{\text{Sem}}$, the intuitive distance is $d(x,y) = ||x-y||_{L^2}$. Our experiments with cross-validation led to $\gamma = 10$.

However, for the application on the *visual* signatures of size $X = 100$: $\mathscr{S} = \mathscr{S}_{\text{Vis}}$ and the $X \times X = 10,000$ coefficients of the transformation matrix W should be positive in order to maintain the positiveness of visual word frequencies. Besides, as our sample size is relatively small, there is a risk of overfitting if all the $10,000$ coefficients of W are involved in the optimization process. For this reason, we only consider the optimization of diagonal matrices W, which amounts to optimize $K = 100$ visual word weights. Finally, the χ^2 pseudo-distance, initially used between visual word signatures, is an intuitive distance $d(.,.)$ between the transformed visual word signatures which should be L^1-normalized before χ^2 measures are performed:

$$d(W\ \mathscr{S}_{\text{Vis}}(I), W\ \mathscr{S}_{\text{Vis}}(J)) = \chi^2\left(\frac{W\ \mathscr{S}_{\text{Vis}}(I)}{||W\ \mathscr{S}_{\text{Vis}}(I)||_{L^1}}, \frac{W\ \mathscr{S}_{\text{Vis}}(J)}{||W\ \mathscr{S}_{\text{Vis}}(J)||_{L^1}}\right) \quad (7)$$

Due to the choice of the χ^2 pseudo-distance, the differentiation of the cost function f with respect to W was less straightforward but feasible. We also tried the L^2 distance for the distance

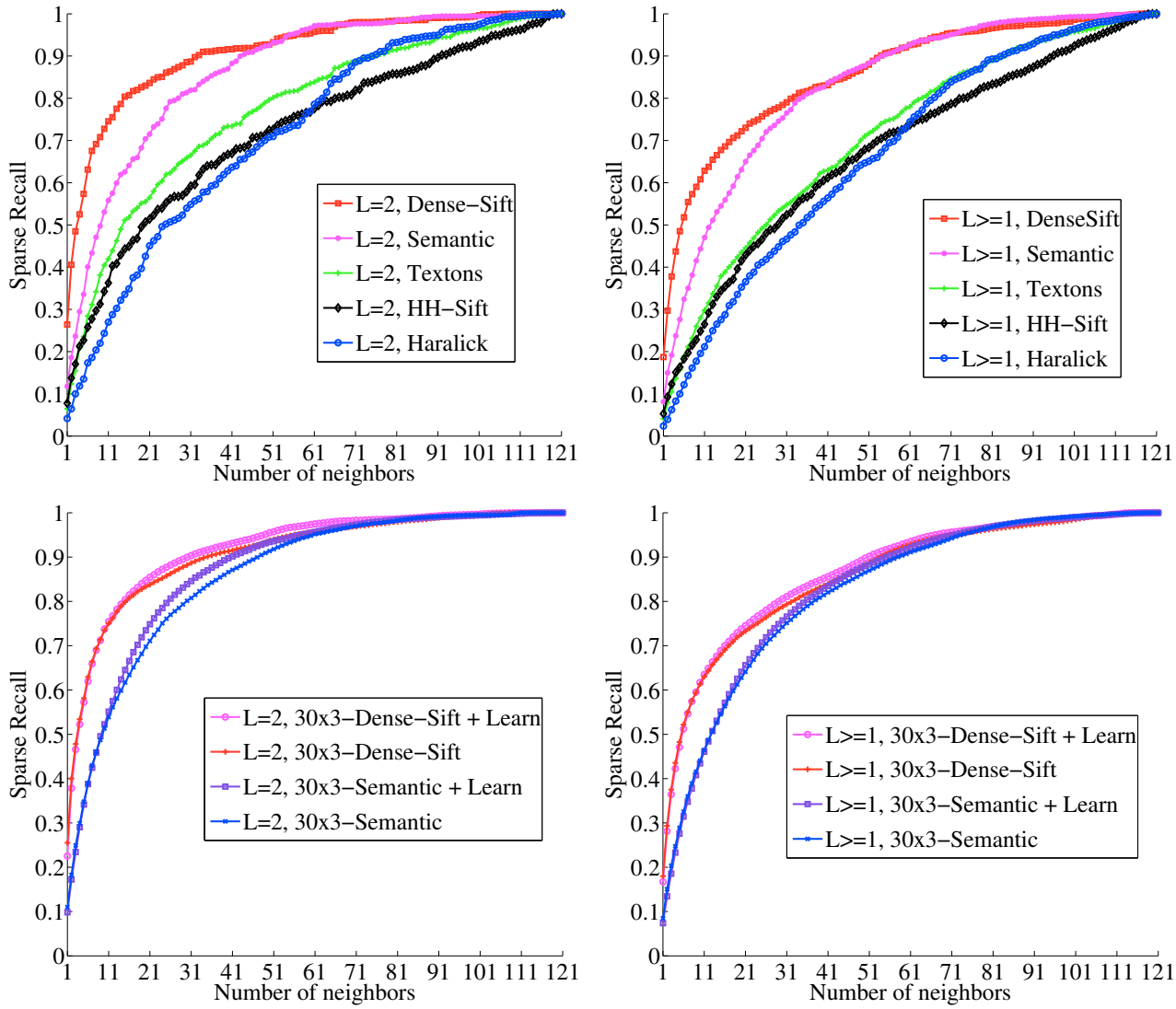

Fig. 6: *Sparse recall* curves associated with the retrieval methods in L-scored domains where $L = +2$ (left) or $L >= 1$ (right). For retrieval methods using distance learning, each *sparse recall* curve is the median of the *sparse recall* curves computed with 30×3 cross-validation. The recall curves associated with "Semantic" and "Semantic + Learn" are indirect indicators of the relevance of the *semantic* signature. As explained in in Section VI-D, the small performance loss observed with the *semantic* signature must not be interpreted as a rejection of the method.

$d(.,.)$ but we did not retain it because the results were not as good as with the χ^2 pseudo-distance. Our experiments with cross-validation for the *visual* signatures also led to $\gamma = 10$.

VI. Evaluation and Results

A. Cross-validation

In order to exclude any learning bias, we used $m \times q$-fold cross-validation, i.e. m random partitions of the database into q subsets. Each of these subsets is successively the testing set and the union of the $q - 1$ others is the training set. To exclude patient-related bias, all videos from the same patient are in the same subset. Given our sparse ground truth for perceived similarity, q must be not too large in order to have enough similarity scores in each testing set, and not too small to ensure enough similarity scores in the training set. For our experiments, we performed $m = 30$ random partitions of our pCLE video database into $q = 3$ subsets. When computing any performance indicator, we will consider as a robust indicator value the median of all the indicator values computed with cross-validation.

B. Retrieval Evaluation Tools

Standard recall curves are a common means of evaluating retrieval performance. However, because of the sparsity of our perceived similarity ground truth, it is not possible to compute them in our case. As an alternative, we define *sparse recall* curves. At a fixed number n of nearest neighbors in the complete video database, we define the *sparse recall* value $\mathrm{SR}(n)$ of a retrieval method as the percentage of L-scored video couples, with $L = +2$ or $L >= 1$, for which one of

the two videos has been retrieved by the method among the n nearest neighbors of the other video:

$$\mathrm{SR}(n) = \frac{\mathrm{Card}\{(x,y) \in E \mid e(x,y) = L, x \in \mathcal{V}_y^n \text{ or } y \in \mathcal{V}_x^n\}}{\mathrm{Card}\{(x,y) \in E \mid e(x,y) = L\}} \quad (8)$$

where E are the edges of the sparse similarity graph $G = (V, E)$, $e(x, y)$ is the similarity score of the edge (x, y) and $\mathcal{V}_x^n$ is the n-neighborhood of the video x. The resulting *sparse recall* curve, for example with $L = +2$, shows the ability of the retrieval method to extract, among the first nearest neighbors, videos that are perceived as *very similar* to the video query.

The evaluation of a retrieval method against perceived similarity ground truth can be qualitatively illustrated by four superimposed histograms $H_L, L \in \{-2, -1, +1, +2\}$. H_L is defined as the histogram of the similarity distances which were computed by the retrieval method in the restricted domain of all L-scored video couples, where L is one of the four Likert points: *very dissimilar* (-2), *rather dissimilar* (-1), *rather similar* $(+1)$ and *very similar* $(+2)$. The more separated these four histograms are, the more likely the distance computed by the retrieval method will be correlated with perceived similarity ground truth. As a separability measure between each pair of histograms, we use the Bhattacharyya distance which is closely related to the Bayes error [29] and thus more indicative of a probability of similarity between histograms than the simple histogram intersection.

C. Evaluation of Semantic Concept Extraction

In order to evaluate, from the semantic point of view, our visual-word-based *semantic* extraction method, we propose to measure the detection performance of each of the $M = 8$ *semantic weights* contained in the *semantic* signature. For the j^{th} semantic concept, we compute a ROC curve that shows the matching performance of the learned *semantic weight* s_j with respect to the semantic ground truth c_j. The obtained ROC curves reflect how well the presence of semantic concepts can be learned from the visual words.

Possible indicators of the correlation between the distance computed by a retrieval method and the perceived similarity ground truth are Pearson correlation π, Spearman ρ and Kendall τ. Compared to Pearson π which measures linear dependence based on the data values, Spearman ρ and Kendall τ are better adapted to the psychometric Likert scale because they measure monotone dependence based on the data ranks [30]. Kendall τ is less commonly used than Spearman ρ but its interpretation in terms of probabilities is more intuitive. To assess statistical significance for the comparison between two correlation coefficients associated with two retrieval methods, we have to perform the adequate statistical test. First, ground-truth data on the four-point Likert scale are characterized by a non-normal distribution, so data ranks should be used instead of data values. Second, the rank correlation coefficients measured for two methods are themselves correlated because they both depend on the same ground-truth data. For these reasons, we decide to perform Steiger's Z-tests, as recommended by Meng et al. [31], and we apply it to Kendall τ.

D. Results and Discussions

For our experiments, we compared the retrieval performances of "Dense-Sift" with those of "HH-Sift", "Haralick" and "Textons" presented in Section III which are considered as state-of-the-art in CBIR. We call "Semantic" the visual-word-based *semantic* retrieval method, "30x3-Semantic" the same method with 30×3 cross-validation and "30x3-Dense-Sift" the "Dense-Sift" with 30×3 cross-validation. "30x3-Semantic+Learn" (resp. "30x3-Semantic+Learn") is the "30x3-Semantic" method (resp. "30x3-Dense-Sift+Learn" method) improved with distance learning.

In terms of *sparse recall* performances, we observe in Fig. 6 that the retrieval methods from best to worst are: "Dense-Sift+Learn", "Dense-Sift", "Semantic+Learn", "Semantic", "Textons", "HH-Sift" and "Haralick". According to the recall associated with $L = +2$, our "Dense-Sift" method based on the *visual* signatures is able to capture, within the 10 first neighbors, more than 70% of the video couples perceived as "very similar", which is quite encouraging for our retrieval application. We also observe that perceived similarity distance learning allows to slightly improve recall performance. The fact that "Dense-Sift" outperforms "Semantic" in terms of recall performance, before and after distance learning, is due to the drastic dimensionality reduction which was performed by our Fisher-based transformation, from $K = 100$ visual words to $M = 8$ semantic concepts. Indeed, *semantic* signatures seem to be too short to discriminate *very similar* video pairs as well as *visual* signatures. Although the recall results based on *semantic* signatures are not as good as those based on *visual* signatures, the curve of *semantic* signatures is much closer to the curve of *visual* signatures than the curves of state-of-the-art methods. We can therefore be rather confident in the fact that the *semantic* signatures are informative. *Sparse recall* is only a means to evaluate the relevance of the *semantic* signatures. Ultimately, we want to base the retrieval of pCLE videos on visual content and not on semantic annotations, otherwise the retrieval system might retrieve videos that are semantically related but not similar in appearance, in which case the physician might lose trust in the retrieval system.

On the superimposed histograms shown in Figs. 7 and 8, we qualitatively observe that "Dense-Sift" and "Semantic" globally better separate the four histograms than "HH-Sift", "Haralick" and "Textons", and that perceived similarity distance learning allows to better separate the histogram H_{+2} from the other histograms. These observations are quantitatively confirmed by the Bhattacharyya distances shown in Table II. The correlation results shown in Table III also confirm these findings and demonstrate that, with statistical significance, the similarity distances computed by "Dense-Sift" and "Semantic" are better correlated with the perceived similarity than the similarity distances computed by "HH-Sift", "Haralick" and "Textons". Besides this, the learned similarity distances are with statistical significance better correlated with the perceived similarity than the original distances. These results also show

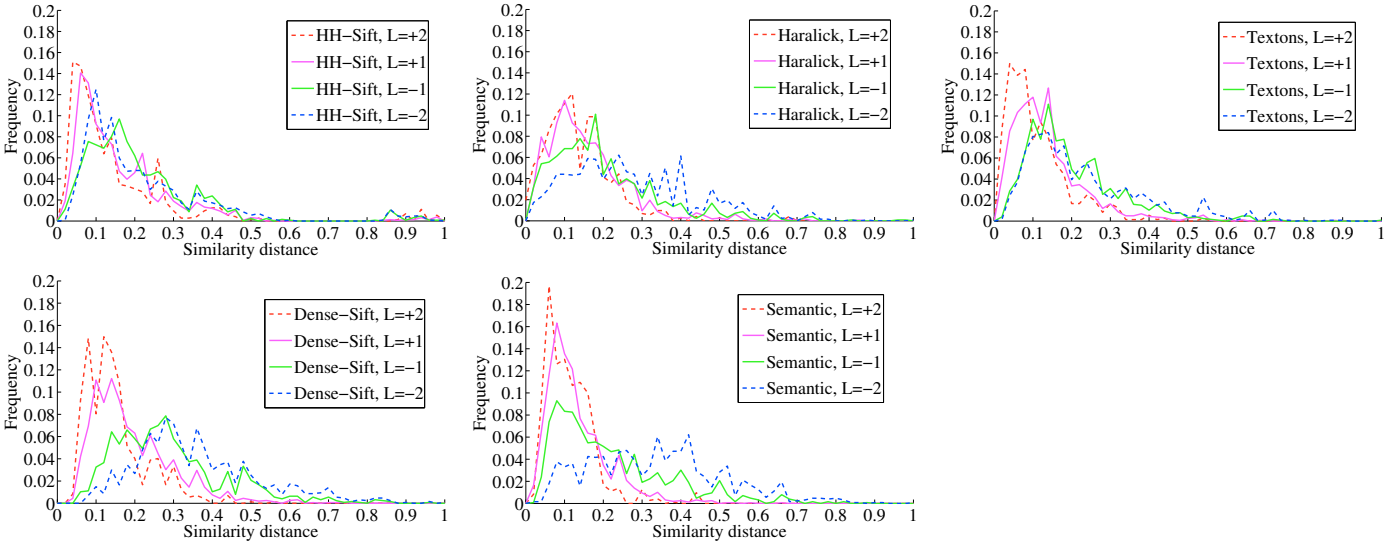

Fig. 7: Superimposed histograms H_L of the similarity distances in each L-scored domain. On the top from left to right: "HH-Sift" method, "Haralick" method, "Textons" method. On the bottom from left to right: "Dense-Sift" method, "Semantic" method.

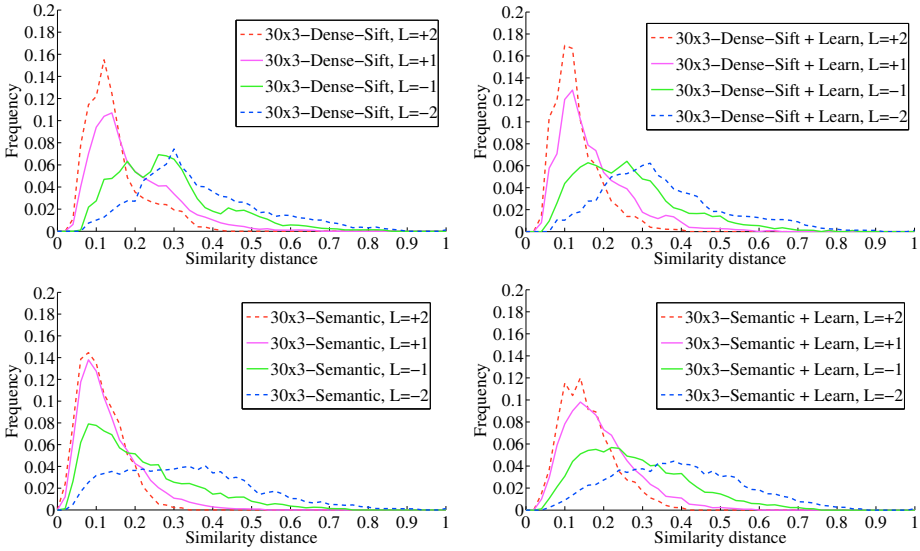

Fig. 8: Superimposed histograms H_L of the similarity distances in each L-scored domain. On the top: "30x3-Dense-Sift" method (left) and "30x3-Dense-Sift+Learn" method (right). On the bottom: "30x3-Semantic" method (left) and "30x3-Semantic+Learn" method (right). Each histogram is the median of the histograms computed with 30×3 cross-validation.

Bhattacharyya distance between Hist(L) and Hist(L')	$L=+2$ $L'=+1$	$L=+2$ $L'=-1$	$L=+2$ $L'=-2$	$L=+1$ $L'=-1$	$L=+1$ $L'=-2$	$L=-1$ $L'=-2$
10x3-Sem+Learn	0.024	0.175	0.468	0.078	0.294	0.072
10x3-Sem	0.018	0.145	0.441	0.071	**0.299**	**0.075**
10x3-DS+Learn	**0.036**	**0.236**	**0.500**	**0.087**	0.254	0.047
10x3-DS	0.030	0.205	0.412	0.084	0.219	0.036
Semantic (Sem)	0.046	0.200	**0.571**	0.090	**0.352**	**0.102**
Dense-Sift (DS)	**0.051**	**0.257**	0.519	**0.096**	0.251	0.051
Textons	0.030	0.152	0.193	0.067	0.095	0.023
Haralick	0.042	0.089	0.206	0.038	0.125	0.048
HH-Sift	0.037	0.098	0.102	0.047	0.042	0.027

TABLE II: Measures of separability, using Bhattacharyya distance, between the four L-scored histograms H_L shown in Figs 7 and 8 for each retrieval method. For the retrieval methods using 30×3 cross-validation, we computed the median of the Bhattacharyya distances.

Retrieval method M	**M1"** 10x3-Sem+Learn	**M1'** 10x3-Sem	**M2"** 10x3-DS+Learn	**M2'** 10x3-DS	**M1** Sem	**M2** DS	**M3** Textons	**M4** Haralick	**M5** HH-Sift
Pearson π	55.7 %	53.3 %	53.4 %	51.4 %	54.6 %	51.6 %	35.3 %	35.4 %	15.8 %
σ	0.3 %	0.2 %	0.2 %	0.2 %					
Spearman ρ	56.6 %	53.8 %	58.2 %	55.5 %	55.3 %	55.7 %	38.2 %	34.5 %	22.8 %
σ	0.3 %	0.2 %	0.2 %	0.3 %					
Kendall τ	50.9 %	48.1 %	**52.4** %	49.8 %	49.4 %	**50.0** %	34.1 %	30.4 %	20.0 %
σ	0.3 %	0.2 %	0.2 %	0.2 %					
Steiger's Z-test on τ; p-value	**> M1'** $p = 0.022$		**> M1'** **> M2'** $p < 0.003$		**> M3,M4 > M5** $p < 10^{-45}$	**> M3,M4 > M5** $p < 10^{-60}$	**> M4 > M5** $p < 10^{-4}$	**> M5** $p < 10^{-15}$	
	$\sim$ M2",M2' $p > 0.05$	**$\sim$ M2'** $p = 0.163$	**$\sim$ M1"** $p > 0.05$		**$\sim$ M2** $p = 0.486$				

TABLE III: Indicators of correlation between the similarity distance computed by the retrieval methods and the ground truth. For the retrieval methods using 30×3 cross-validation, we show the median of correlation coefficients. The standard deviation σ of each correlation estimator can be computed from the standard deviation of the n samples $\sigma_{samples} = \sqrt{n-1}\sigma$. We also show the median of p-values when comparing two retrieval methods using 30×3 cross-validation. **> M** indicates that the improvement from method **M** is statistically significant, **$\sim$ M** indicates that it is not.

that the correlation performance of "30x3-Semantic+Learn" (resp. "30x3-Semantic") is comparable to that of "30x3-Dense-Sift+Learn" (resp. 30x3-Dense-Sift"), as their difference is not statistically significant.

From the semantic point of view, the performance of the *semantic* signature can be appreciated in the ROC curves shown in Fig. 9. Each ROC curve associated with a concept c_j is the median of the ROC curves computed with 30×3 cross-validation by thresholding on the *semantic weight* s_j. According to the areas under the ROC curves (AUC) shown in Table IV, the semantic concepts, from the best classified to the worst classified, are: *elongated crypt*, *round crypt*, *abnormal nuclei density*, *abnormal nuclei*, *normal goblet cell*, *lumen*, *blood vessel* and *star-shaped opening*. The fact that the concept *elongated crypt* is very well classified shows that the visual words clearly express whether this concept is present or not in pCLE videos. As the presence of elongated crypts in a pCLE video is a typical criterion of malignancy for the endoscopists, we deduce that *semantic* signatures could be successfully used for pCLE classification between malignant and non-malignant colonic polyps. Although the concepts *blood vessel* and *star-shaped opening* are poorly classified, they contribute, as "weak classifiers", to the clinical relevance of the whole *semantic* signature because their ROC curves are above the diagonal. As the semantic detection deriving from *semantic* signatures is based on a rather intuitive Fisher-based linear method, it is worth to be compared with more sophisticated classification method, such as Support Vector Machines (SVM). We thus test the detection performance of a linear SVM and a non-linear SVM based on radial basis functions, which we feed with the visual word signatures. The resulting ROC curves are shown in Figs. 10 and 11. Each ROC curve associated with a concept c_j is the median of the ROC curves computed with 30×3 cross-validation. In order to assess the statistical significance of AUC differences, we used the non-parametric method of DeLong et al. [32] based on the Mann-Whitney U-statistic. From the AUC values in Table IV we deduce that most of the ROC curves obtained with the linear SVM and with the non-linear SVM are statistically worse than those obtained with our intuitive method, and none of them are statistically better. More precisely, our method outperforms the linear SVM method with statistical significance for all semantic concepts except the concept $c4$. Compared to the non-linear SVM method, our method performs also better for all semantic concepts except $c4$, and statistical significance is demonstrated for the concepts $c1$, $c2$, $c3$ and $c5$. These AUC comparison results demonstrate the relevance of our intuitive Fisher-based method in terms of semantic detection, and thus the relevance of the *semantic* signatures.

In order to ensure both the high recall of the visual-word-based retrieval including perceived similarity learning, and the clinical relevance of the semantic information contained in the *semantic* signature, we propose a pCLE retrieval system where the most similar videos are extracted using the "Dense-Sift+Learn" method, and where the star plots representing *semantic* signatures are displayed as additional information. Fig. 12 shows some typical results of our pCLE retrieval system with 5 nearest neighbors, with the added semantic ground truth represented by underlined concepts. In clinical practice, the semantic ground truth is not known for the video query, but in these retrieval examples it is disclosed for illustration purposes. The extracted pCLE videos, represented as mosaic images, look quite similar in appearance to the query, the first neighbor being more visually similar than the 5^{th} one. On each star plot, the font size of each written semantic concept is proportional to the normalized value of its *semantic weight*. Semantic concepts written in large characters may or may not be in agreement with the underlined concepts present in the ground truth. Most importantly, if for a given pCLE video, the semantic ground truth is very different from the estimated *semantic* signature, then the difficulty to interpret the video for diagnosis purpose might be high, because visual content is not correlated with semantic annotations. Our visual-word-based *semantic* signature would thus have the potential to distinguish ambiguous from non-ambiguous pCLE videos. The remaining disagreements between the learned semantic information and the semantic ground truth show that, even though we have achieved encouraging results in extracting

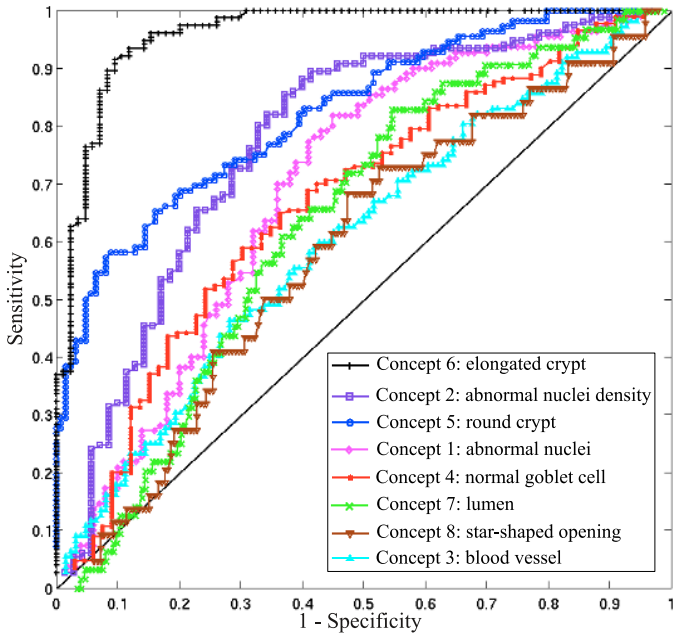

Fig. 9: ROC curves showing the semantic detection performance obtained from our intuitive Fisher-based method, by thresholding on the *semantic* signatures.

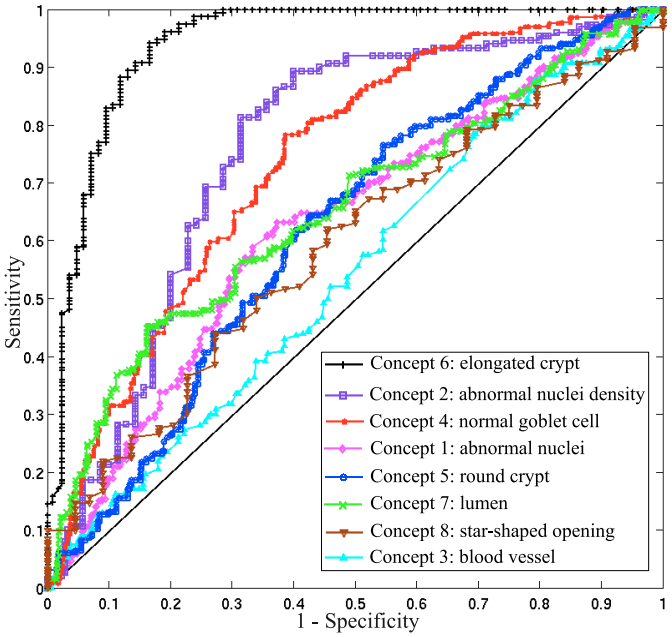

Fig. 10: ROC curves showing the semantic detection performed by non-linear SVM (based on radial basis functions) fed with the visual word signatures.

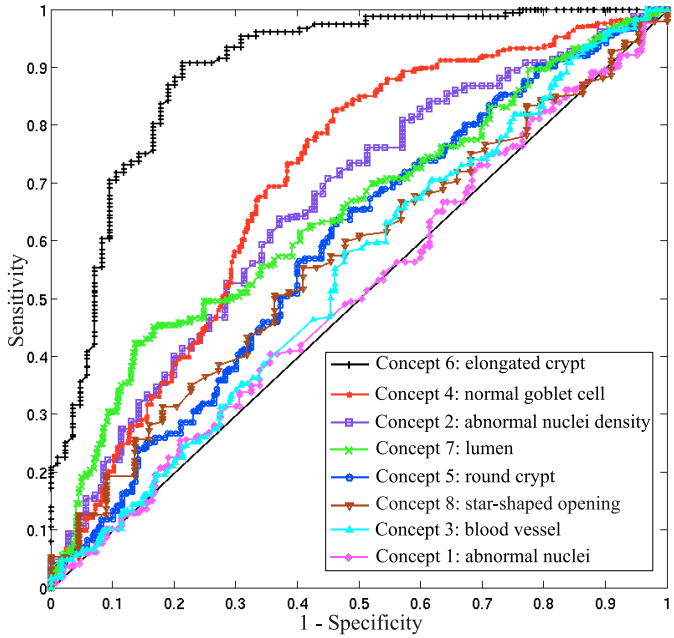

Fig. 11: ROC curves showing the semantic detection performed by a linear SVM fed with the visual word signatures.

Semantic concept	**AUC Linear SVM**	**AUC Non-Linear SVM**	**AUC Our method**
c1. abnormal nuclei	51.4 %	62.9 %	75.6 %
c2. abnormal nuclei density	65.8 %	75.7 %	81.8 %
c3. blood vessel	53.6 %	55.0 %	66.2 %
c4. normal goblet cell	69.8 %	73.6 %	71.6 %
c5. round crypt	58.9 %	62.0 %	86.3 %
c6. elongated crypt	89.6 %	94.2 %	96.7 %
c7. lumen	64.7 %	65.5 %	68.6 %
c8. star-shaped opening	57.0 %	59.4 %	62.8 %

TABLE IV: Area under the ROC curves (AUC) for each detection method according to each semantic concept.

semantics from visual words, further investigations are still needed to bridge the semantic gap between low-level visual features and high-level clinical knowledge.

VII. Conclusion

The pCLE retrieval system proposed in this study provides the endoscopists with clinically relevant information, both visual and semantic, that should be easily interpretable to make an informed pCLE diagnosis. While *visual* signatures are employed to extract visually similar pCLE videos, *semantic* signatures are used to complement the retrieval results with pCLE semantic estimations. Our main contributions are: (1) a Fisher-based method that builds short visual-word-based *semantic* signatures, (2) an intuitive representation of these *semantic* signatures using star plots, (3) the creation of an on-line tool to generate a relevant ground truth for visual similarity perceived by multiple endoscopists between pCLE videos, (4) a method for distance learning from perceived visual similarity to improve retrieval relevance, and (5) the implementation of several tools to evaluate retrieval methods, such as correlation

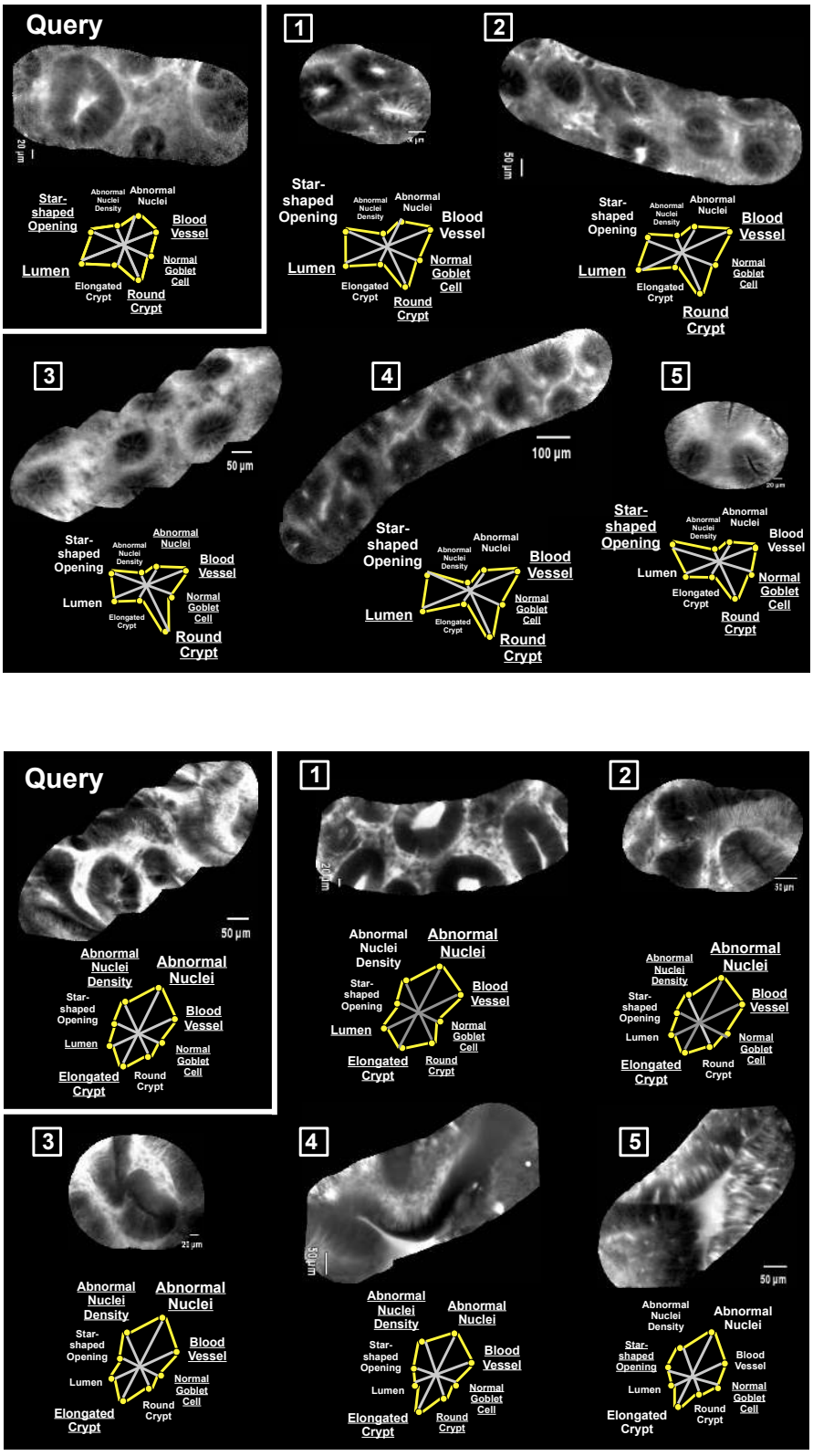

Fig. 12: Examples of pCLE retrieval results from a non-neoplastic video query (top) or a neoplastic video query (bottom). The 5 most similar videos are retrieved by "30x3-Dense-Sift+Learn" method. For each video, the star plot representation of its *semantic* signature is provided. The font size of each written semantic concept is proportional to the value of the concept coordinate in the star plot. Underlined concepts are those which were annotated as present in the semantic ground truth. In practice, the semantic ground truth is not known for the video query, but it is disclosed here for illustration purposes. For illustration purposes, videos are represented by mosaic images.

measures and *sparse recall* curves. Moreover, this proposed methodology could be applied to other medical or non-medical databases, as long as ground-truth data are available.

Despite our relatively small pCLE database and despite the sparsity of the perceived similarity ground truth, our evaluation experiments show that the visual-word-based *semantic* signatures extract, from low-level visual features, a higher-level clinical knowledge which is consistent with respect to perceived similarity. Possible disagreements between the semantic estimation, based on visual features, and the semantic ground truth could be investigated in order to estimate the interpretation difficulty of pCLE videos, which we explored in a previous study [33] only based on visual words. Future work will focus on more sophisticated methods to learn jointly visual and semantic similarity. Our long-term objective is the clinical evaluation of our visual-semantic retrieval system to see whether it could help the endoscopists in making more accurate pCLE diagnosis.

REFERENCES

[1] H. Müller, J. Kalpathy-Cramer, C. E. Kahn, W. Hatt, S. Bedrick, and W. R. Hersh, "Overview of the ImageCLEFmed 2008 medical image retrieval task," in *CLEF*, 2008, pp. 512–522. 1

[2] U. Avni, H. Greenspan, E. Konen, M. Sharon, and J. Goldberger, "X-ray categorization and retrieval on the organ and pathology level, using patch-based visual words," *IEEE Trans. Med. Imag.*, vol. 30, no. 3, pp. 733–746, 2011. 1

[3] A. W. M. Smeulders, M. Worring, S. Santini, A. Gupta, and R. Jain, "Content-based image retrieval at the end of the early years," *IEEE Trans. Pattern Anal. Mach. Intell.*, vol. 22, no. 12, pp. 1349–1380, 2000. 2

[4] C. B. Akgül, D. L. Rubin, S. Napel, C. F. Beaulieu, H. Greenspan, and B. Acar, "Content-based image retrieval in radiology: Current status and future directions," *J. Digital Imaging*, vol. 24, no. 2, pp. 208–222, 2011. 2

[5] O. Khalid, S. Radaideh, O. W. Cummings, M. J. O' Brien, J. R. Goldblum, and D. K. Rex, "Reinterpretation of histology of proximal colon polyps called hyperplastic in 2001," *World J Gastroenterol*, vol. 15, no. 30, pp. 3767–70, 2009. 2

[6] B. André, T. Vercauteren, M. B. Wallace, A. M. Buchner, and N. Ayache, "Endomicroscopic video retrieval using mosaicing and visual words," in *Proc. ISBI'10*, 2010, pp. 1419–1422. 2, 4

[7] B. André, T. Vercauteren, A. M. Buchner, M. B. Wallace, and N. Ayache, "Retrieval evaluation and distance learning from perceived similarity between endomicroscopy videos," in *Proc. MICCAI'11*, 2011, pp. 289–296. 2, 3

[8] ——, "Learning semantic and visual similarity for endomicroscopy video retrieval," INRIA, INRIA Technical Report RR-7722, Aug. 2011. [Online]. Available: http://hal.inria.fr/inria-00618057/en/ 2

[9] A. M. Buchner, M. W. Shahid, M. G. Heckman, M. Krishna, M. Ghabril, M. Hasan, J. E. Crook, V. Gomez, M. Raimondo, T. Woodward, H. Wolfsen, and M. B. Wallace, "Comparison of probe based confocal laser endomicroscopy with virtual chromoendoscopy for classification of colon polyps," *Gastroenterology*, vol. 138, no. 3, pp. 834–842, 2009. 3

[10] T. Vercauteren, A. Perchant, G. Malandain, X. Pennec, and N. Ayache, "Robust mosaicing with correction of motion distortions and tissue deformation for in vivo fibered microscopy," *Med. Image Anal.*, vol. 10, no. 5, pp. 673–692, Oct. 2006. 3

[11] E. Dabizzi, M. W. Shahid, B. Qumseya, M. Othman, and M. B. Wallace, "Comparison between video and mosaics viewing mode of confocal laser endomicroscopy (pCLE) in patients with Barrett's esophagus," *Gastroenterology (DDW 2011)*, 2011. 3

[12] VSS, "Visual similarity scoring (VSS)," http://smartatlas.maunakeatech.com, login: MICCAI-User, password: MICCAI2011. 3

[13] R. Kiesslich, J. Burg, M. Vieth, J. Gnaendiger, M. Enders, P. Delaney, A. Polglase, W. McLaren, D. Janell, S. Thomas, B. Nafe, P. R. Galle, and M. F. Neurath, "Confocal laser endoscopy for diagnosing intraepithelial neoplasias and colorectal cancer in vivo," *Gastroenterology*, vol. 127, no. 3, pp. 706–13, 2004. 4

[14] J. Zhang, S. Lazebnik, and C. Schmid, "Local features and kernels for classification of texture and object categories: a comprehensive study," *Int. J. Comput. Vis.*, vol. 73, pp. 213–238, Jun. 2007. 4

[15] T. Leung and J. Malik, "Representing and recognizing the visual appearance of materials using three-dimensional textons," *Int. J. Comput. Vis.*, vol. 43, pp. 29–44, Jun. 2001. 4

[16] F.-F. Li and P. Perona, "A Bayesian hierarchical model for learning natural scene categories," in *Proc. CVPR'05*, 2005, pp. 524–531. 4

[17] R. M. Haralick, "Statistical and structural approaches to texture," in *Proc. IEEE*, vol. 67, 1979, pp. 786–804. 4

[18] GLCM texture features, http://www.mathworks.com/matlabcentral/fileexchange/22187-glcm-texture-features. 4

[19] A. Oliva and A. Torralba, "Modeling the shape of the scene: A holistic representation of the spatial envelope," *Int. J. Comput. Vis.*, vol. 42, no. 3, pp. 145–175, 2001. 4

[20] B. Poblete, B. Bustos, M. Mendoza, and J. M. Barrios, "Visual-semantic graphs: using queries to reduce the semantic gap in web image retrieval," in *Proc. ACM Information and Knowledge Management*, 2010, pp. 1553–1556. 5

[21] H. Ma, J. Zhu, M. R. Lyu, and I. King, "Bridging the semantic gap between image contents and tags," *IEEE Trans. Multimedia*, vol. 12, pp. 462–473, 2010. 5

[22] J. C. Caicedo, J. G. Moreno, E. A. Niño, and F. A. González, "Combining visual features and text data for medical image retrieval using latent semantic kernels," in *Proc. Multimedia Information Retrieval*, 2010, pp. 359–366. 5

[23] N. Rasiwasia, P. J. Moreno, and N. Vasconcelos, "Bridging the gap: Query by semantic example," *IEEE Trans. Multimedia*, vol. 9, no. 5, pp. 923–938, 2007. 5

[24] N. Rasiwasia, J. C. Pereira, E. Coviello, G. Doyle, G. R. G. Lanckriet, R. Levy, and N. Vasconcelos, "A new approach to cross-modal multimedia retrieval," in *ACM Multimedia*, 2010, pp. 251–260. 5

[25] R. Kwitt, N. Rasiwasia, N. Vasconcelos, A. Uhl, M. Häfner, and F. Wrba, "Learning pit pattern concepts for gastroenterological training," in *Proc. MICCAI'11*, 2011, pp. 273–280. 5

[26] L. Yang, R. Jin, L. Mummert, R. Sukthankar, A. Goode, B. Zheng, S. C. H. Hoi, and M. Satyanarayanan, "A boosting framework for visuality-preserving distance metric learning and its application to medical image retrieval," *IEEE Trans. Pattern Anal. Mach. Intell.*, vol. 32, pp. 30–44, 2010. 5

[27] K. Q. Weinberger and L. K. Saul, "Distance metric learning for large margin nearest neighbor classification," *J. Mach. Learn. Res.*, vol. 10, pp. 207–244, 2009. 5

[28] J. Philbin, M. Isard, J. Sivic, and A. Zisserman, "Descriptor learning for efficient retrieval," in *Proc. ECCV'10*, 2010, pp. 677–691. 5

[29] T. Kailath, "The divergence and Bhattacharyya distance measures in signal selection," *IEEE Trans. Commun. Technol.*, vol. 15, no. 1, pp. 52–60, 1967. 8

[30] V. Barnett, *Sample Survey principles and methods*. Hodder Arnold, 1991. 8

[31] X.-L. Meng, R. Rosenthal, and D. B. Rubin, "Comparing correlated correlation coefficients," *Psychological Bulletin*, vol. 111, no. 1, pp. 172–175, 1992. 8

[32] E. R. DeLong, D. M. DeLong, and D. L. Clarke-Pearson, "Comparing the areas under two or more correlated receiver operating characteristic curves: a nonparametric approach," *Biometrics*, vol. 44, no. 3, pp. 837–845, 1988. 10

[33] B. André, T. Vercauteren, A. M. Buchner, M. W. Shahid, M. B. Wallace, and N. Ayache, "An image retrieval approach to setup difficulty levels in training systems for endomicroscopy diagnosis," in *Proc. MICCAI'10*, no. 6362, 2010, pp. 480–487. 13